Bulletin of Geophysics and Oceanography Vol. XX, n. X, pp. XXX-XXX; Xxxxx 20xx
DOI 10.4430/bgo00493

On the capability of multilayer perceptron to predict total organic carbon and elemental capture spectroscopy data in unconventional hydrocarbon reservoirs: the case of the Barnett Shale and Bakken oil field

L. Aliouane[1] and S.-A. Ouadfeul[2]

[1] *Earth Physics Laboratory, M'Hamed Bougara University, Boumerdes, Algeria*
[2] *Direction Centrale Recherche et Développement, Sonatrach, Boumerdes, Algeria*

(Received: 20 July 2023; accepted: 22 May 2025; published online: 10 July 2025)

ABSTRACT This study explores the capability of a Multilayer Perceptron (MLP) neural network (NN) machine to predict missing or expensive core rocks and well-log data measurements such as the Total Organic Carbon (TOC) and Elemental Capture Spectroscopy (ECS) measurements. Data of boreholes drilled in the Lower Barnett Shale and Bakken oil and gas fields, located in the USA, are used. TOC estimation is first addressed using the Schmoker method in the Barnett Shale gas and Bakken oil reservoirs, followed by the implementation of MLP NNs trained with various learning algorithms such as the Hidden Weight Optimisation, the Conjugate Gradient, and the Levenberg-Marquardt. Input data include standard well logs such as sonic, gamma ray, resistivity, and neutron porosity. The MLP models are validated and generalised using both horizontal and vertical well data. Furthermore, ECS data prediction is performed using MLPs trained on elementary analysis-derived log parameters, offering a cost-effective alternative to direct ECS logging. The results demonstrate that the efficiency and reliability of MLP-based approaches in enhancing geochemical and petrophysical characterisation of subsurface formations is conditioned by the choice of the learning algorithm, the reservoir complexity, number of wells, and their distribution.

Key words: TOC, ECS, prediction, MLP, learning algorithms, HWO, LVM, CG, Barnett Shale, Bakken Oil.

1. Introduction

Reservoir characterisation using Artificial Intelligence (AI) and Machine Learning (ML) has become a hot topic of research, in the last decade. El-Dabaa *et al.* (2024) published a paper dealing with the use of an unsupervised ML-based multi-attribute analysis for enhancing gas channel detection and facies classification in the Serpent field, offshore the Nile Delta, Egypt. Goliatt *et al*. (2023) discussed the performance of evolutionary optimised ML for modelling Total Organic Carbon (TOC) in core samples of shale gas fields. The obtained results show that, regardless of the metaheuristic used to guide the model selection, optimised extreme learning machines attained the best performance scores according to six metrics. Such hybrid models can be used in exploratory geological research, particularly for unconventional oil and gas resources. Ismail *et al*. (2021) paper deals with the problem of gas channel and chimney prediction using

© 2025 - The Author(s)

artificial neural networks (ANNs) and multi-seismic attributes and its application to the offshore West Nile Delta, located in Egypt. Longman *et al*. (2024) paper discusses the exploratory analysis of ML methods for TOC prediction using well-log data of the Kolmani field. Saporetti *et al*. (2022) published a paper that shows different hybrid ML models for estimating TOC from mineral constituents in core samples of shale gas fields. The results obtained proved that ML methods, assisted by the evolutionary algorithm, could accurately estimate TOC and be used to carry out further exploratory geological analyses, especially those related to the prospects of unconventional oil-gas resources.

The Multilayer Perceptron (MLP) ANN model has been widely used in the last decades as predictor in the full spectrum of sciences (Awadallah, 2023). Fierro *et al*. (2022) showed an application of a single MLP model to predict the solubility of carbon dioxide in different ionic liquids for gas removal processes. Fujita *et al*. (2019) used the MLP model to create a prediction model for dressing independence in a small sample at a single facility suggesting that higher accuracy could be expected with a MLP rather than with logistic regression and decision-tree strategy when creating a prediction model for the independence of daily-life activities in a small sample of stroke patients. In geophysics and geology, the MLP is used to estimate electrical resistivity. For this purpose, a case study from the Lublin basin, located in SE of Poland, is shown (Ważny *et al*., 2021). The authors of this paper used five separate MLP models that were trained on subsequent chronostratigraphic intervals. Waszkiewicz *et al*. (2019) estimated the absolute permeability using a MLP ANN based on well logs and laboratory data from Silurian and Ordovician deposits in SE of Poland; the obtained results show the legitimacy of using ANNs in the issue of estimating permeability. However, they also show limitations resulting from the lack of accurate data or influence of geological setting and processes. Ouadfeul and Aliouane (2012) demonstrated that the MLP neural network is not suitable to predict lithofacies in case of small numbers of input-output couples, i.e. the case of core rock data, since they are expensive. To resolve this drawback, the authors of the paper suggested a combination between the Kohonen self-organising map and the MLP.

In this paper, the capability of the MLP ANN to predict missing or expensive well-log data, such as the TOC and the Elemental Capture Spectroscopy (ECS) data, is tested in boreholes drilled in the Barnett Shale and Bakken oil fields. The following three learning algorithms were used: the Hidden Weight Optimisation (HWO), Conjugate Gradient (CG), and Levenberg-Marquardt (LM). This paper is organised as follows: an initial description of the theory and methods, a discussion of the results obtained, and, ultimately, the conclusions.

2. Materials and methods

This section is organised as follows: to start, a definition of the TOC and the Schmoker method that uses the density well log to estimate TOC and, then, a description of the principal of the ECS well-logging tool that measures the mineralogy content of different geological formations crossed by a borehole. Next, the problem of TOC prediction using the MLP ANN with different learning algorithms, in Bakken oil and Barnett Shale field data, is discussed. Following, a debate of the problem of ECS data prediction using the MLP ANN in the Bakken Oil field. Numap, CG and LM-MLP software, developed by Neural Decision Research Laboratory, are used for the implementation of MLP machines [for more details on the software see https://www.neuraldl.com/Software.php; for more information on the HWO, CG, and LM training algorithms see Yu and Manry (2002), Azami *et al*. (2013), and Aliouane *et al*. (2014)].

2.1. MLP

The neurons of a MLP can be seen as a multitude of perceptrons connected to each other. The topological particularity of this network is that all the neurons of a layer are connected to all the neurons of the next layer. Each neuron, therefore, has *N* inputs, where *N* is the number of neurons present in the previous layer, and an output that is sent to all the neurons of the next layer. Each neuronal connection is associated with a weight, *W,* as for the inputs of the perceptron. The calculation of a neuron output is made according to the activation function chosen. Many activation functions are proposed in literature, among which the Sigmoid is one of the most popular; for more details about the MLP and activation functions see Gardner and Dorling (1998)]:

$$Sig(X) = \frac{1}{(1+e^{-x})}. \tag{1}$$

A major advantage of the MLP is its singular nature and its flexibility to adjust to different binary problems. However, the best performance can be obtained when MLPs are used for classification and prediction with a supervised learning mechanism. The most suitable form of data for MLPs is simply a tabular data set with labels assigned to input signals. Throughout the development of ML techniques, MLPs found their place as a basic neural model at the preliminary recognition stage of analysis but also as a versatile predictive tool (Ważny *et al*., 2021)

2.2. TOC prediction using a MLP ANN

TOC, with no unit to quantify it, is the amount of organic carbon in a source rock. A high TOC (> 5%) is very important to identify good shale plays and sweet spots. Three methods are used for TOC measurement and estimation. The first method is based on direct measurement in laboratory; the second method is based on direct measurement using a well-logging tool, and the last method is based on empirical measurement. In the case of this study, two methods are used: the Passey (Passey *et al*., 2010) and the Schmoker methods. The Schmoker method was developed in Devonian shales using bulk density logs (Schmoker, 1979, 1980) and was later refined in Bakken shales (Schmoker, 1983). Based on the response of the bulk density measurement to low-density organic matter (~1.0 g/cm^3), the Schmoker method, as it is commonly called, computes TOC as follows (Schmoker, 1980):

$$TOC = \frac{154.497}{\rho_b} - 57.261 \tag{2}$$

where ρ_b is the bulk density in g/cm^3 and TOC is reported in wt%. This equation assumes a constant mineral composition and porosity throughout the formation. Although the method was developed and refined based on specific environments, it is frequently used for TOC estimation in a wide variety of shale formations (Ouadfeul and Aliouane, 2015a, 2015b).

2.2.1. Application to the Barnett Shale and Bakken oil fields

In this section, the TOC well log is predicted in three horizontal wells, i.e. 1H, 2H, and 3H, using a MLP ANN. These wells are drilled in the Lower Barnett Shale gas reservoir, which is located in the USA. The two horizontal wells, 1H and 3H, are used for the learning and validation phases whereas the horizontal well, 2H, is used for generalisation. Fig. 1 shows the location map of the Barnett Shale and Fig. 2 shows the top of the Upper and Lower Barnett Shale and the trajectory of the three horizontal wells. To predict TOC, a MLP machine composed of one hidden layer is implemented. Of utmost importance is the fact that one hidden layer is enough to resolve such problem (Ouadfeul and Aliouane, 2015b). The MLP machine is composed of three neurons in the input layer and one neuron in the output layer. The number of neurons in the input layer is equal to the number of well logs that are used as input. The well-log data are: P-wave slowness, S-wave slowness, and natural gamma ray. The number of neurons in the output layer is equal to the number of the predicted well logs using the implemented MLP machine. In this case, only one log is predicted. The number of neurons in the hidden layer is determined after many numerical experiences. For each experience, the root-mean-square- error (RMSE) is calculated and the number of neurons in the hidden layer providing the lowest root mean square (RMS) is chosen. Fig. 3 shows the graphs of the well-log data that are used as input of the MLP machine. Track number 2 of Fig. 4 shows the Schmoker TOC log for horizontal wells 1H and 3H, respectively. This log is used as a desired output for the learning and validation phases. As a general rule, before the application of AI, a quality control of the different data must be performed and to do this the histogram of each log is calculated with the goal of checking data distribution and removing abnormal values and depth intervals containing gaps. Table 1 shows the minimum and maximum values of different well-log data for horizontal wells 1H, 2H, and 3H, respectively.

The result analysis demonstrates that data are ready for the application of AI. The hidden layer is composed of 50 neurons; this number is obtained after 645 numerical experiences. The RMSE between the desired and calculated outputs using a MLP machine with 50 neurons in the hidden layer is equal to 0.05, being this RMS value lower compared to the RMS value of other machines with different neuron numbers in the hidden layer. The implemented machine is trained in a supervised mode using the HWO learning algorithm and, at this stage, 60% of the

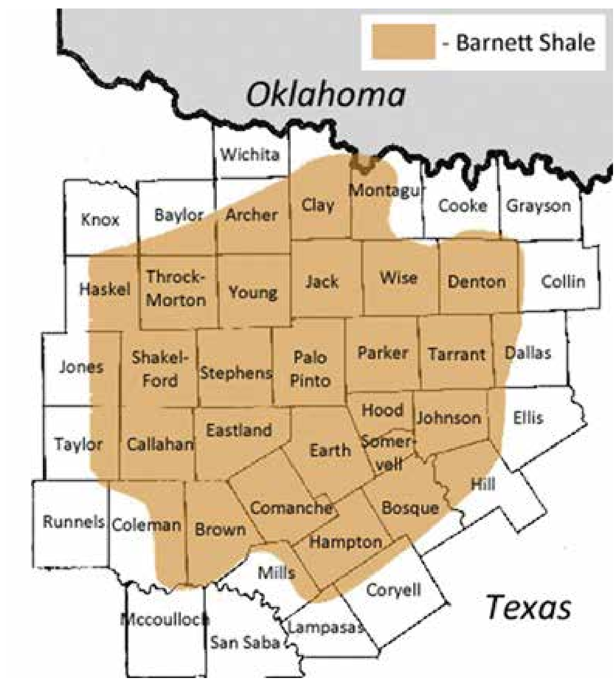

Fig. 1 - Location map of the Barnett Shale (Universal Royalty Company, 2013).

input-output couples is used for the training phase and 40% is used for the validation phase. Data of horizontal well 2H are used for the generalisation phase. Fig. 5 shows the slowness log of P and S waves, and the natural gamma ray, recorded in this well. These data are propagated through the implemented MLP machine with the connection weights optimised during the learning phase. Fig. 6 shows the following logs for well 2H: the Schmoker TOC, the predicted TOC using the implemented MLP machine, and their difference.

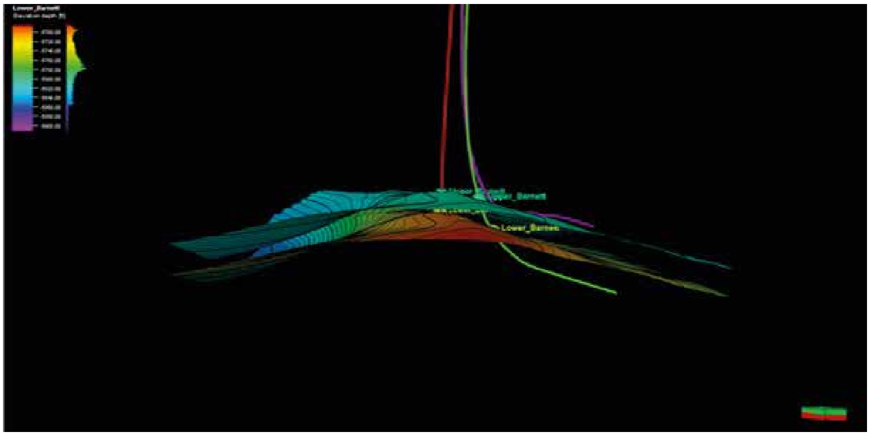

Fig. 2 - The top and bottom of the Lower Barnett Shale gas reservoir and the trajectory of horizontal wells 1H (red), 2H (magenta), and 3H (green).

The second phase consists in checking the capability of the MLP to predict TOC in vertical wells that cross the Bakken oil source rock. Fig. 7 shows the location map of the Bakken formation and Fig. 8 shows the seismic surfaces of the top and bottom of this source rock along with the trajectory of four vertical wells named OLSON 13-26, ORTLOFF 13-28, THOMPSON 1-4, and WALLEN 1. Fig. 9 shows the recorded raw well-log data in the four boreholes, which are: deep and shallow resistivity, P-wave slowness, and neutron porosity. As done before, the minimum and maximum values of these data and Schmoker TOC derived from the density log are calculated. Table 2 shows the global values for the four wells cited above. The analysis of these values shows that the deep resistivity logs contain high values, which are due to the presence of spikes. To overcome this phenomenon, a despiking operation, is performed prior to the application of AI. The data of the two boreholes, OLSON 13-20 and ORTLOFF 13-28, are used for the training and validation phases, while the data of boreholes THOMPSON 1-4 and WALLEN 1 are used for the generalisation phase. A MLP ANN machine with one hidden layer is trained in a supervised mode and the CG learning algorithm is used; the number of neurons in the hidden layer is equal to 40. The data of the two boreholes are divided into two parts: 60% are used for the training phase and 40% are used for the validation phase. Fig. 10 shows the following logs of boreholes OLSON 13-20 and ORTLOFF 13-28: Schmoker TOC, TOC predicted during the learning and validation phases using the implemented MLP machine, and the difference between these two logs. Fig. 11 shows the same logs for boreholes THOMPSON 1-4 and WALLEN 1, but the predicted TOC is obtained in the generalisation phase of the implemented machine. During the generalisation phase the raw well-log data, recorded in these boreholes (shown in Fig. 9), are propagated through the implemented MLP machine, using the weights of connections optimised during the learning and validation phases.

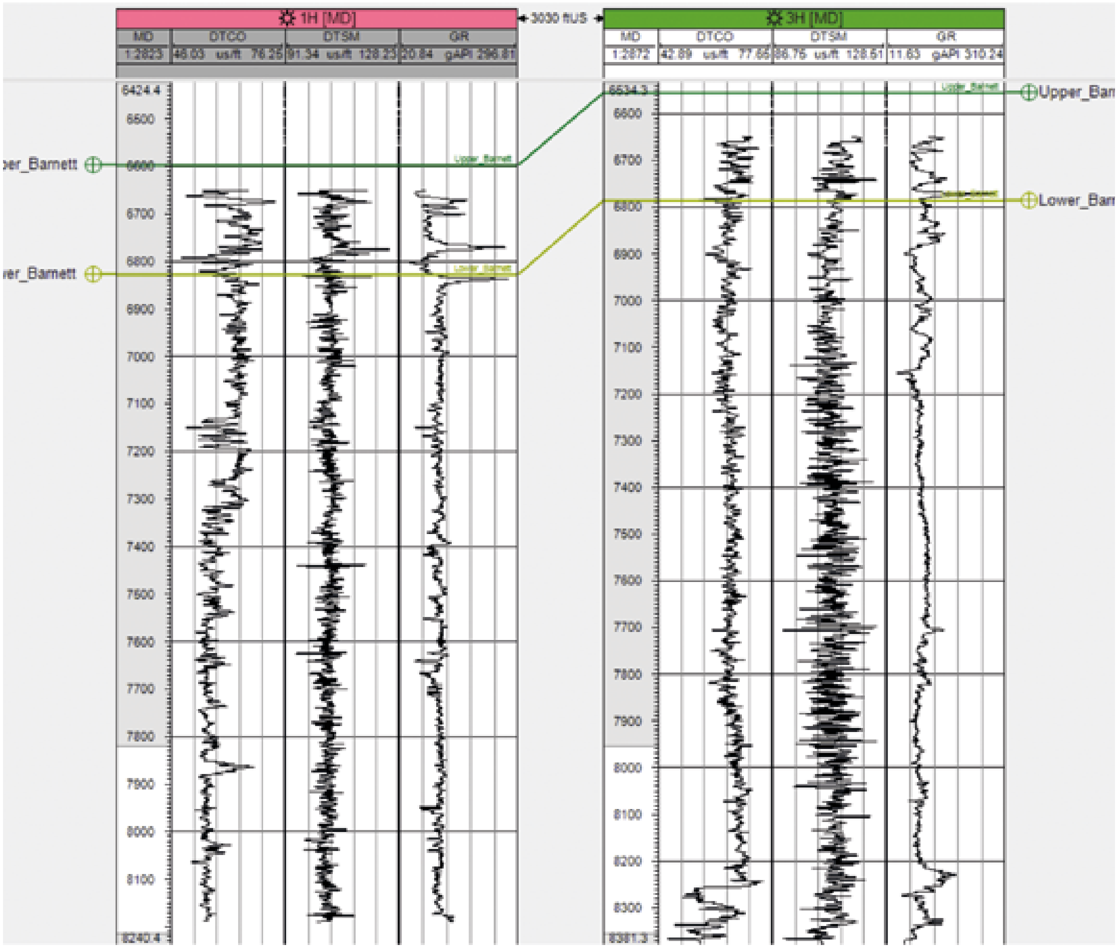

Fig. 3 - Raw well-log data used as input of the implemented MLP machine; track 1: measured depth, track 2: P-wave slowness, track 3: S-wave slowness, and track 4: natural gamma ray.

Table 1 - Maximum and minimum values of the well-log natural gamma ray, P-wave slowness, S-wave slowness, and Schmoker TOC derived from the density log; for horizontal wells 1H, 2H, and 3H.

Well	Log	Min	Max
1H	Gr	40	280
1H	DTCO	48	74
1H	DTSM	94	126
1H	Schmoker TOC	-1.5	8.5
2H	Gr	15	120
2H	DTCO	47.22	63.33
2H	DTSM	90.91	108.42
2H	Schmoker TOC	-0.5	8.1
3H	Gr	36.51	285.35
3H	DTCO	45.97	74.76
3H	DTSM	90.27	125.03
3H	Schmoker TOC	-1.0	17.62

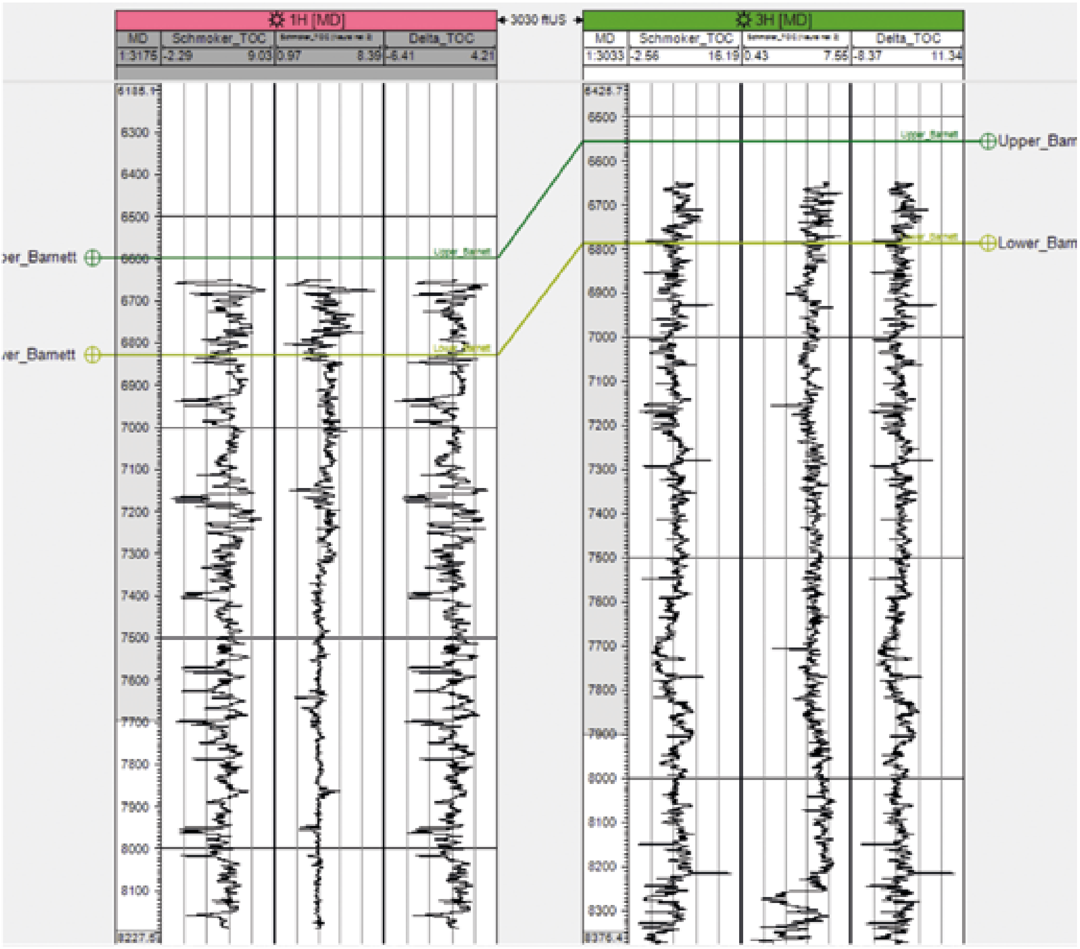

Fig. 4 - Graphs of Schmoker TOC, predicted TOC using the HWO training algorithm, and their difference in horizontal wells 1H and 3H; track 1: measured depth, track 2: Schmoker TOC used as a desired output to train the MLP machine, track 3: obtained TOC using MLP with HWO training algorithm, and track 4: the difference.

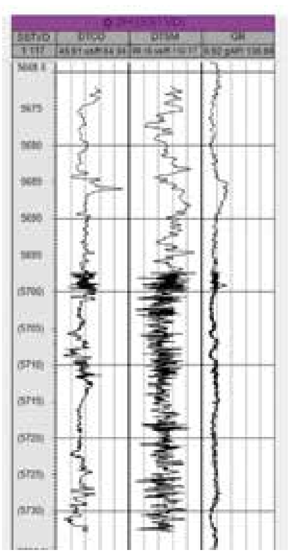

Fig. 5 - Well-log data of horizontal well 2H. These data are used as input of the implemented MLP machine for the generalisation phase; track 1: measured depth, track 2: P-wave slowness, track 3: S-wave slowness, and track 4: natural gamma ray.

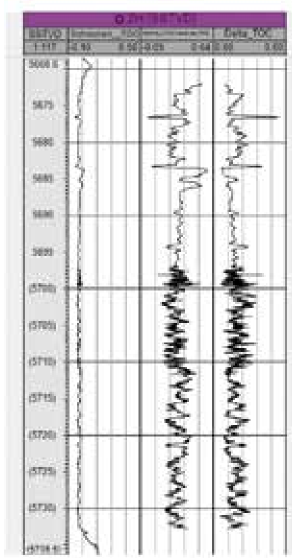

Fig. 6 - TOC logs and their difference in horizontal well 2H; track 1: measured depth, track 2: Schmoker TOC, track 3: predicted TOC using the implemented MLP machine with HWO training algorithm, and track 4: the difference.

Fig. 7 - Location map of the Bakken formation (Vatter *et al.*, 2022).

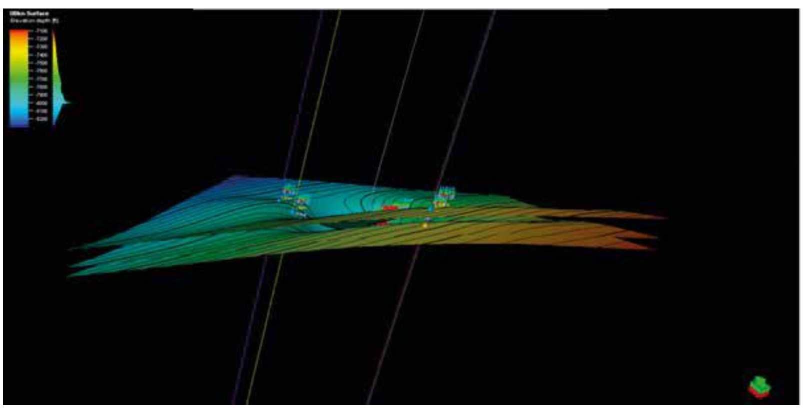

Fig. 8 - Top of Upper Bakken, Lower Bakken and Three Forks, and the trajectory of the following vertical wells: OLSON 13-26 (red), ORTLOFF 13-28 (yellow), THOMPSON 1-4 (magenta), and WALLEN 1 (blue).

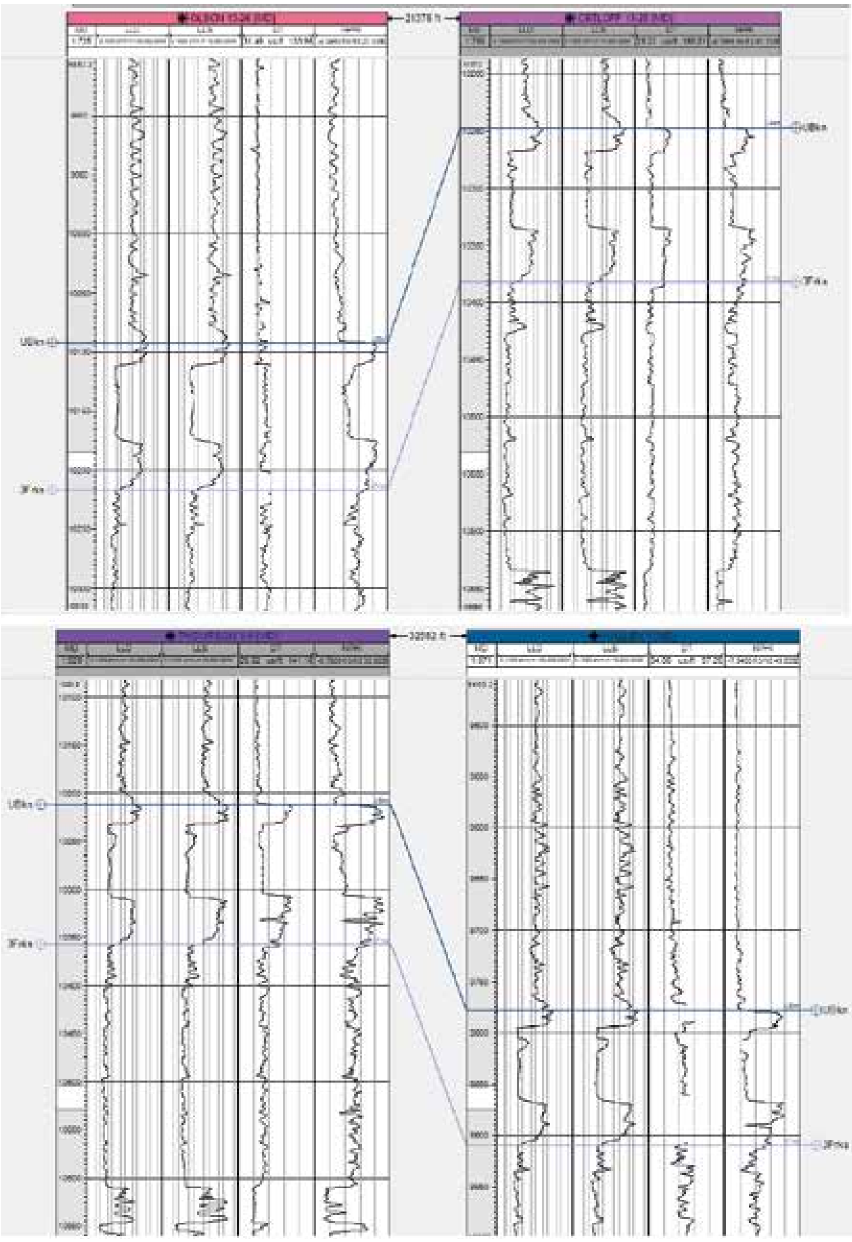

Fig. 9 - Raw well-log data recorded in boreholes OSLON 13-26, ORTLOFF 13-28, THOMPSON-1, and WALLEN 1; track 1: measured depth, track 2: deep resistivity, track 3: shallow resistivity, track 4: P-wave slowness, and track 5: neutron porosity.

Table 2 - Global minimum and maximum values of the log resistivity of the shallow and deep zones, P-wave slowness, neutron porosity, and Schmoker TOC derived from the density log, for the four boreholes, OSLON 13-26, ORTLOFF 13-28, THOMPSON-1, and WALLEN 1.

Log	Min	Max
LLS	0.20	2148.90
LLD	0.19	91593
DT	1.29	176.80
NPHI	-2.78	60.48
Schmoker TOC	-0.1	10.9

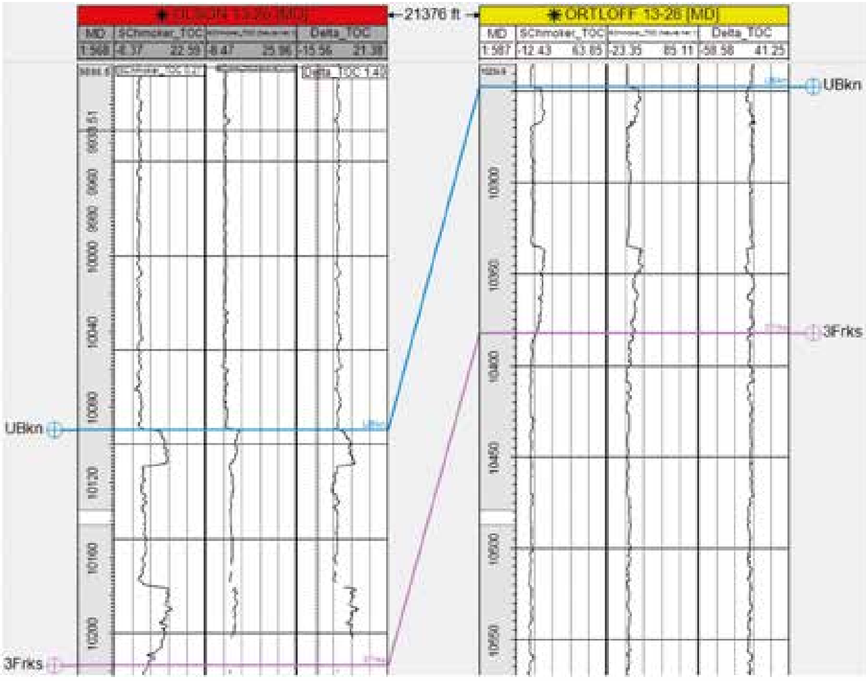

Fig. 10 - TOC logs and their difference in boreholes OLSON 13-20 and ORTLOFF 13-28, the predicted TOC log is obtained in the learning and validation phases; track 1: measured depth, track 2: Schmoker TOC, track 3: obtained TOC using MLP with CG training algorithm, and track 4: the difference.

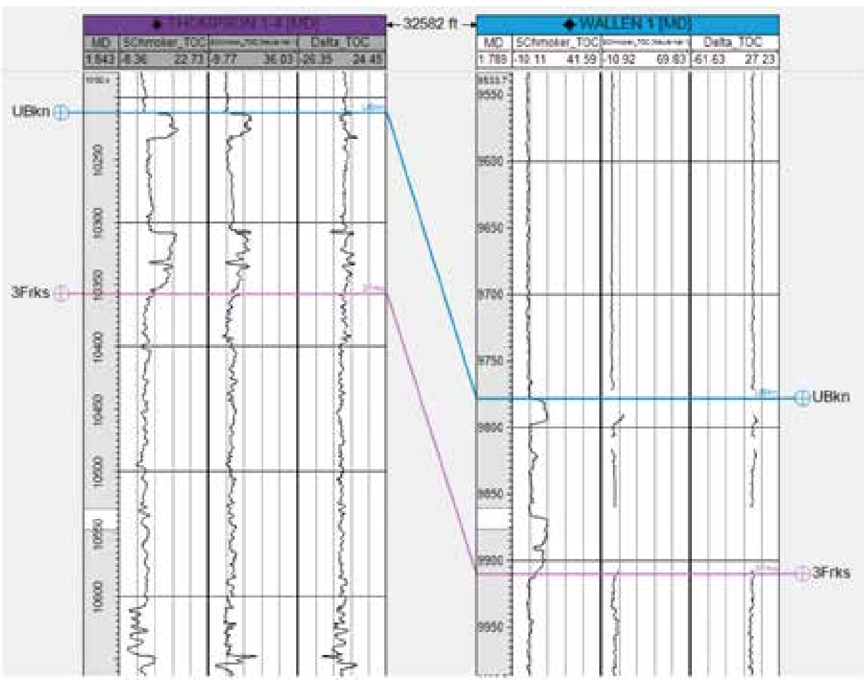

Fig. 11 - TOC logs and their difference in horizontal wells THOMPSON 1-4 and WALLEN 1, the predicted TOC log is obtained in the generalisation phase; track 1: measured depth, track 2: Schmoker TOC, track 3: obtained TOC using MLP with CG training algorithm, and track 4: the difference.

2.3. ECS data prediction using a MLP ANN

2.3.1. The ECS sonde

The ECS sonde, which is a small and easy-to-use logging tool, measures and processes gamma ray spectra, or the number of gamma rays, received by the detector at specific energy levels. These measurements allow for a more accurate definition of the clay content, mineralogy, and matrix properties of each potential zone. Using the neutron-induced capture gamma ray spectroscopy principle, the ECS sonde determines relative elemental yields by measuring the gamma rays produced when neutrons bombard the formation and lose energy as they are scattered, primarily by hydrogen [for more details about the ECS sonde see Schlumberger (2006)].

2.3.2 Application to the Bakken oil field

In this section, the capability of the MLP ANN to predict ECS data in vertical wells drilled in the Bakken oil field is tested and data of two boreholes, NS41X-36H and NS42X-36H, are used. The goal is to avoid direct measurement with the ECS tool inside the boreholes as it is very expensive. The results of Elemental Analysis (ELAN), using the raw well logs, are used as input, while the measured ECS tool data are used as output. Fig. 12 shows the ELAN data for wells NS41X-36H and NS42X-36H. The ELAN data correspond to: 1) water volume in the invaded zone, 2) water volume in the deep zone, 3) quartz volume, 4) irreducible water saturation, 5) illite volume, and 6) clay volume.

Fig. 13 shows the ECS data of borehole NS41X-36H. These data are used as a desired output of the implemented MLP machine, in the training and validation phases. The figure also shows the ECS data of borehole NS42X-36H, which are used for the generalisation phase of the implemented MLP machine. The measured ECS data inside these two boreholes are: 1) permeability, 2)

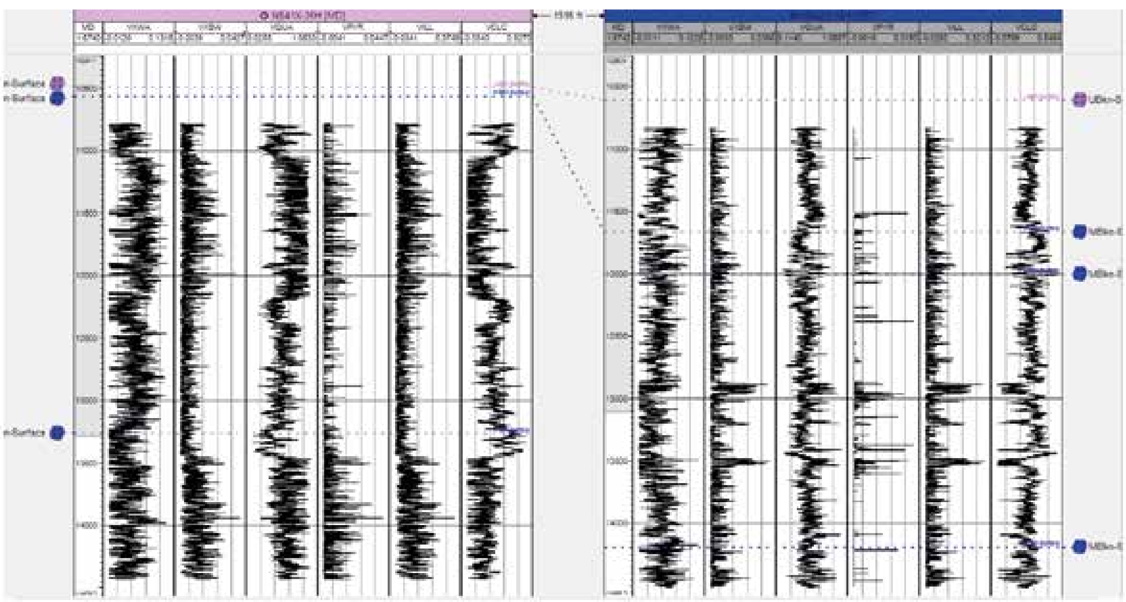

Fig. 12 - ELAN data for wells NS41X-36H and NS42X-36H used as input to train and test the MLP machine; track 1: measured depth, track 2: water volume in the invaded zone, track 3: water volume in the deep zone, track 4: quartz volume, track 5: irreducible water, track 6: illite volume, and track 7: clay volume.

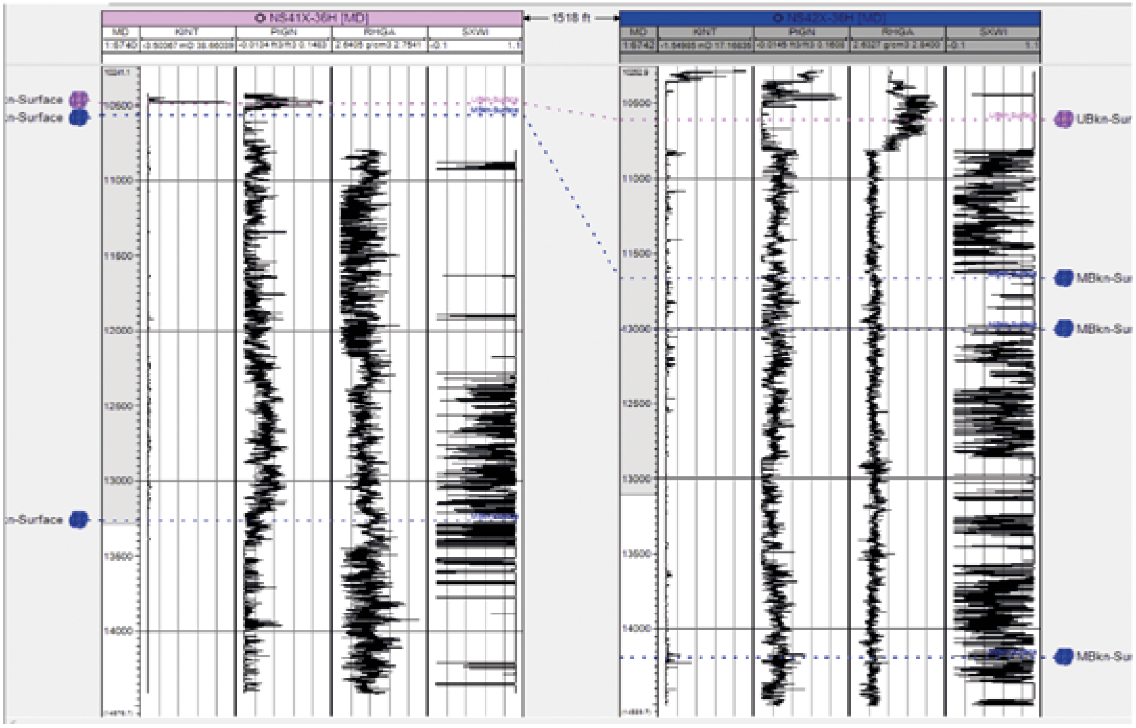

Fig. 13 - ECS data that will be used to implement the MLP machine of wells NS41X-30H (training and validation phases) and NS42X-36H (generalisation phase); track 1: measured depth, track 2: permeability, track 3: effective porosity, track 4: bulk density, and track 5: saturation of irreducible water.

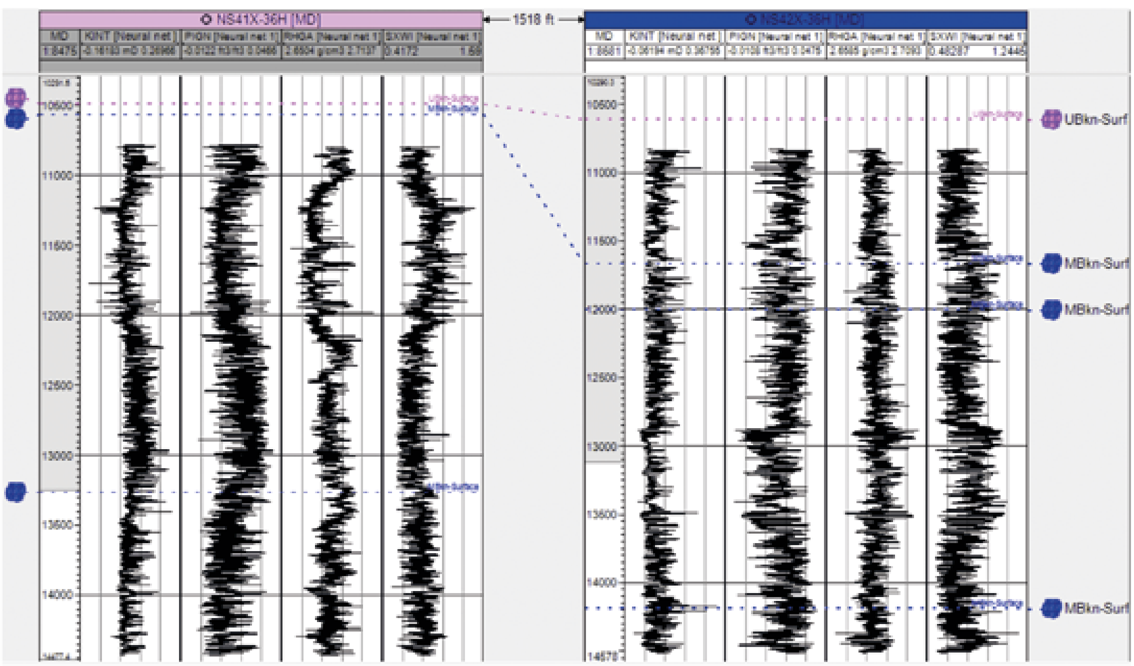

Fig. 14 - Predicted ECS data using the implemented MLP with the LM training algorithm for wells NS41X-36H (training and validation phases) and NS42X-36H (generalisation phase); track 1: depth, track 2: effective porosity, track 3: bulk density, and track 4: saturation of irreducible water.

Table 3 - Minimum and maximum ELAN and ECS merged well-log data values for boreholes NS41X-36H and NS42X-36H.

Log	Min	Max
VXWA	0.	0.11
VXBW	0.	0.06
VQUA	0.	0.98
VPYR	0.	0.14
VILL	0.	0.54
VCLC	0.	0.95
KINT	0.01	474.96
PIGN	0.0001	0.23
RHGA	2.31	2.84
SXWI	0.	1.

effective porosity, 3) bulk density, and 4) saturation of irreducible water. To check data quality, before AI application, maximum and minimum ELAN and ECS merged well-log data values are calculated (see Table 3 for obtained values). The result analysis demonstrates that these data are suitable for AI application. The LM learning algorithm is used to train the implemented MLP machine, composed of three layers. The input layer is composed of 6 neurons, the hidden layer is composed of 200 neurons (obtained after 700 numerical experiences), and the output layer is composed of 4 neurons. During the learning and validation phases, the ELAN-ECS couple data of borehole NS41X-36H were used to optimise the weights of the connections between neurons. To evaluate the learning and validation phases of the implemented machine, the ELAN data of borehole NS41X-36H are propagated through the implemented machine, using the optimised weights of the connections; Fig. 14 shows the output of the implemented machine. To evaluate the generalisation phase, the ELAN data of borehole NS42X-36H are propagated through the machine; Fig. 14 also shows the predicted ECS of the generalisation phase.

3. Results and discussion

The RMSE, derived from the Delta_TOC log (shown in Fig. 4), is the summation of the square of the Delta_TOC for all the full depths, devided by the number of samples containing the full depth. The Correlation Coefficient (CC) between two logs (Log1 and Log2) is the slope of the linear regression of the set of points obtained by cross-plotting Log2 versus Log1.

The RMSE between the predicted TOC log, using the implemented MLP machine and the calculated TOC logs using the Schmoker model for horizontal wells 1H and 3H (presented in Fig. 4), is equal to 0.05 and the CC is equal to 97%. These good results reflect good learning of the implemented MLP machine. Using the same procedures, the CC and RMSE between the predicted and calculated TOC are calculated for horizontal well 2H (generalisation phase). The CC is equal to 88% and the RMSE is equal to 0.43. These values reflect the ability of the implemented MLP machine to predict the TOC log.

The CC between the calculated and predicted TOC for boreholes OLSON 13-20 and ORTLOFF 13-28, and the RMSE (presented in Fig. 10), obtained during the learning and validation phases, are equal to 90% and 0.20, respectively. These results confirm good learning of the implemented MLP machine during these two phases.

However, the CC between the predicted and Shmoker TOC logs for boreholes THOMPSON 1-4 and WALLEN 1 (presented in Fig. 11), obtained in the generalisation phase, drops to 82.5%. The RMSE is equal to 0.9. This quality drop in the results is caused by lateral heterogeneity of the Bakken oil source rock.

During the learning and validation phases, the CC between the measured and predicted ECS logs for borehole NS41X-30H (presented in Fig. 14) is equal to 90% and the RMSE is equal to 0.36. These two values reflect good learning of this machine. The CC between the measured and predicted ECS logs of borehole NS42X-36H (shown in Fig. 14) drops to 70% during the generalisation phase, and the RMSE increases to 1.4. The increase of the RMSE and the drop of the CC are mainly caused by the high heterogeneity of the petrophysical properties of the Bakken oil field.

It is important to highlight that these results do not represent a general rule and cannot always be used to resolve the problem of TOC and ECS data prediction from raw and ELAN well-log data, recorded in shale gas and shale oil reservoirs. The obtained results only represent a case study from the Barnett Shale and Bakken oil fields. This paper presents an important piece of research for the scientific community, since it shows the contribution of AI, such as a MLP ANN, to predict TOC in two huge unconventional hydrocarbon fields such as the Barnett Shale and Bakken Oil. To our best knowledge, this is the first paper, dealing with the topic of ECS data prediction from ELAN data.

4. Conclusions

In this study, we have developed and validated an AI framework based on MLP ANNs to predict critical geochemical parameters, namely, TOC and ECS data, using conventional well-log measurements as input. The methodology was applied to two representative shale plays in North America: the Barnett and Bakken formations. These formations, known for their heterogeneity and complex depositional environments, present significant challenges for traditional petrophysical modelling approaches.

By training the models on horizontal and vertical wells and validating them against independent wells, we have shown that the proposed approach exhibits strong learning capabilities, with high correlation coefficients and low prediction errors across different well trajectories. However, during the generalisation phase, the quality of these metrics drops compared to the learning phase. This can be justified by the geological complexity, diagenesis, and high lateral variation of the Lower Barnett and Bakken oil formations.

Moreover, the use of ECS data, which are typically acquired through expensive and specialised tools, can be effectively substituted through this ML approach, thereby, significantly reducing exploration and production costs without compromising interpretative quality. The metrics that are used for the evaluation of MLP machines for TOC prediction are also used for the assessment of the implemented MLP machine for ECS estimation. These metrics exhibit the same behaviour as those of the first MLP machine. These results demonstrate that the quality of the output depends on the choice of learning algorithms, data volume or number of wells that are used during the learning and validation phases, distribution of wells and the distances between them.

The broader implication of this work lies in its potential to revolutionise how unconventional reservoirs are evaluated and developed. The integration of ML into geophysical workflows provides a pathway towards real-time, data-driven decision-making in reservoir characterisation. Furthermore, the methodology is scalable and adaptable to other basins and target properties;

this research contributes not only to the advancement of shale reservoir evaluation but also to the growing field of digital geoscience, where AI serves as a catalyst for innovation and operational efficiency.

Future work may explore the integration of additional data types such as seismic attributes, image logs, or core-derived mineralogy to further enhance predictive performance. Likewise, using big data and incorporating uncertainty quantification frameworks within the ANN architecture could offer more reliable risk assessments during the decision-making process in hydrocarbon exploration and production.

Acknowledgments. The authors would like to thank the Earth Physics Laboratory of the University of Boumerdes for providing well-log data and for allowing them to publish these data. The authors would also like to express their gratitude to the editor and the anonymous reviewers for their comments, which greatly improved the manuscript.

REFERENCES

Aliouane L., Ouadfeul S-A., Djarfour N. and Boudella A.; 2014: *Permeability prediction using artificial neural networks. A comparative study between back propagation and Levenberg-Marquardt learning algorithms.* In: Pardo-Igúzquiza E., Guardiola-Albert C., Heredia J., Moreno-Merino L., Durán J.J., Vargas-Guzmán J.A. (eds), Mathematics of Planet Earth, Springer, Berlin, Germay, pp. 653-657, doi: 10.1007/978-3-642-32408-6_142.

Awadallah M., Abu-Doush I., Al-Betar M. and Braik M.; 2023: *Metaheuristics for optimizing weights in neural networks.* In: Mirjalili S. and Gandomi A.H. (eds), Comprehensive Metaheuristics, Academic Press, Cambridge, MA, USA, pp. 359-377, doi: 10.1016/B978-0-323-91781-0.00005-3.

Azami H., Malekzadeh M. and Sanei S.; 2013: *A new neural network approach for face recognition based on conjugate gradient algorithms and principal component analysis.* J. Math. Comput. Sci., 6, 166-175.

El-Dabaa S.-A., Metwalli F.-I. and Maher A.; 2024: *Unsupervised machine learning-based multi-attributes analysis for enhancing gas channel detection and facies classification in the Serpent Field, offshore Nile Delta, Egypt.* Geomech. Geophys. Geo-energ. Geo-resour., 10, 185, doi: 10.1007/s40948-024-00907-1.

Fierro E.N., Faúndez C.A., Muñoz A.S. and Cerda P.I.; 2020: *Application of a single multilayer perceptron model to predict the solubility of CO_2 in different ionic liquids for gas removal processes.* Processes, 10, doi: 10.3390/pr10091686.

Fujita T., Sato A., Narita A., Sone T., Iokawa K., Tsuchiya K., Yamane K., Yamamoto Y., Ohira Y. and Otsuki K.; 2019: *Use of a multilayer perceptron to create a prediction model for dressing independence in a small sample at a single facility.* J. Phys. Ther. Sci., 31, 69-74, doi: 10.1589/jpts.31.69.

Gardner M. and Dorling S.; 1998: *Artificial neural networks (the multilayer perceptron) - a review of applications in the atmospheric sciences.* Atmos. Environ., 32, 2627-2636.

Goliatt L., Saporetti C., Oliveira L. and Pereira E.; 2023: *Performance of evolutionary optimized machine learning for modeling total organic carbon in core samples of shale gas fields*. Petrol., 10, 150-164, doi: 10.1016/j.petlm.2023.05.005.

Ismail A., Ewida H.F., Nazeri S., Al-Ibiary M.G. and Zollo A.; 2021: *Gas channels and chimneys prediction using artificial neural networks and multi-seismic attributes, offshore west Nile Delta, Egypt.* J. Petrol. Sci. Eng., 208, doi: 10.1016/j.petrol.2021.109349.

Longman F.S., Balogun H., Ojulari R.O., Olatomiwa O.J., Balarabe H.J., Edeh I.S. and Joshua O.O.; 2024: *Exploratory analysis of machine learning methods for total organic carbon prediction using well-log data of Kolmani Field.* In: IEEE 14th International Conference on Pattern Recognition Systems (ICPRS), London, United Kingdom, doi: 10.1109/icprs62101.2024.10677822.

Ouadfeul S. and Aliouane L.; 2012: *Lithofacies classification using the multilayer perceptron and the self-organizing neural networks.* In: Proc., 19th International Conference, ICONIP 2012, Neural Information Processing, Doha, Qatar, Part V 19, pp. 737-744, doi: 10.1007/978-3-642-34478-7.

Ouadfeul S. and Aliouane L.; 2015a: *Total organic carbon prediction in shale gas reservoirs using artificial intelligence with a comparative study between fuzzy logic and neural network.* In: Proc., 13th International Congress Brazilian Geophysical Society & Expogef, Rio de Janeiro, Brazil, pp. 1390-1393, doi: 10.1190/sbgf2015-276.

Ouadfeul S. and Aliouane L.; 2015b: *Total organic carbon prediction in shale gas reservoirs from well logs data using the multilayer perceptron neural network with Levenberg Marquardt training algorithm: application to Barnett Shale.* Arabian J. Sci. Eng., 40, 3345-3349.

Passey Q., Bohacs K., Esch W., Klimentidis R. and Sinha S.; 2010: *From oil-prone source rock to gas-producing shale reservoir - Geologic and petrophysical characterization of unconventional shale-gas reservoirs.* In: Proc. International Oil & Gas Conference and Exhibition, Beijing, China, doi: 10.2118/131350-MS.

Saporetti C.M., Fonseca D.L., Oliveira L.C., Pereira E. and Goliatt L.; 2022: *Hybrid machine learning models for estimating total organic carbon from mineral constituents in core samples of shale gas fields.* Mar. Pet. Geol., 143, doi: 10.1016/j.marpetgeo.2022.105783.

Schlumberger; 2006: *ECS Elemental Capture Spectroscopy sonde*. <www.slb.com/oilfield>.

Schmoker J.; 1979: *Determination of organic content of Appalachian Devonian shales from formation-density logs.* Am. Assoc. Pet. Geol. Bull., 63, 1504-1537, doi; 10.1306/2F9185D1-16CE-11D7-8645000102C1865D.

Schmoker J.; 1980: *Organic content of Devonian shale in western Appalachian Basin.* Am. Assoc. Pet. Geol. Bull., 64, 2156-2165, doi: 10.1306/2F919756-16CE-11D7-8645000102C1865D.

Schmoker J. and Hester T.; 1983: *Organic Carbon in Bakken Formation, United States portion of Williston Basin*. Am. Assoc. Pet. Geol. Bull., 67, 2165-2174.

Universal Royalty Company; 2013: *History of Barnett Shale*, <www.universalroyaltyco.com/resources/history-barnett-shale/>.

Vatter M., Van Vactor S.A. and Coburn T.C.; 2022: *Price responsiveness of shale oil: a Bakken case study*. Nat. Resour. Res., 31, 713-734, doi: 10.1007/s11053-021-09972-9.

Waszkiewicz S., Krakowska-Madejska P. and Puskarczyk E.; 2019: *Estimation of absolute permeability using artificial neural networks (multilayer perceptrons) based on well logs and laboratory data from Silurian and Ordovician deposits in SE Poland.* Acta Geophys., 67, 1885-1894, doi: 10.1007/s11600-019-00347-6.

Ważny J., Stefaniuk M. and Cygal A.; 2021: *Estimation of electrical resistivity using artificial neural networks: a case study from Lublin Basin, SE Poland.* Acta Geophys., 69, 631-642, doi: 10.1007/s11600-021-00554-0.

Yu C. and Manry M.T.; 2002: *A modified hidden optimization algorithm for feedforward neural networks.* In: Proc. 36th Asilomar Conference on Signals, Systems and Computers, vol. 1, pp. 1034-1038.

Corresponding author: Leila Aliouane
Earth Physics Laboratory, Geophysics Department, Faculty of Hydrocarbons and Chemistry, University M'Hamed Bougara of Boumerdes
Boulevard de l'Independance, Boumerdes 35000, Algeria
Phone: +213 552434986; e-mail: l.aliouane@univ-boumerdes.dz